TECHNICAL PAPER

Seismic Response of the Ground Surface Including Underground Horseshoe-Shaped Cavity

Mehdi Panji [1] ⓘ · Saeed Mojtabazadeh-Hasanlouei [1] · Amirabbas Fakhravar [1]

Abstract

In this paper, the seismic response of elastic homogeneous ground surface was presented in the presence of unlined horseshoe-shaped underground cavities subjected to obliquely propagating incident *SH*-waves by using the time-domain half-plane boundary element method (BEM). The Ricker wavelet was considered for the incident wave function. In the use of the proposed method, the boundary around the tunnel was only required to be discretized. After comparing the results of the present study with existing analytical responses, it was found that the method had good accuracy in modeling horseshoe-shaped tunnels. The responses are presented as two-/three-dimensional diagrams in the time/frequency domain. Also, a comparative study is carried out between circular and horseshoe cross-sections to observe the effect of the geometry on the response pattern. The results show that the existence of subsurface openings as well as horseshoe-shaped cavities has a significant effect on the variation of seismic patterns and critical states of the ground surface. The used method can be proposed to geotechnical engineers for preparing simple underground models to achieve the transient responses.

Keyword Horseshoe-cavity, · Half-plane BEM, · *SH*-wave, · Surface response, · Time-domain

✉ Mehdi Panji
m.panji@iauz.ac.ir

Saeed Mojtabazadeh-Hasanlouei
mojtabazadeh@iauz.ac.ir

Amirabbas Fakhravar
fakhravar@iauz.ac.ir

[1]   Department of Civil Engineering, Islamic Azad University, Zanjan Branch, Zanjan, Iran

⧖ Springer

1 Introduction

Study on the behavior of ground surface in the presence of underground cavities is one of the most important studies for constructing any surface structures. In this regard, various methods have been referred for seismic analysis of topographic features and determination of the ground surface responses. In general, seismic analysis methods of topographic features have been divided into three categories including analytical, semi-analytical, and numerical approaches (Panji et al. 2013). In the analytical and semi-analytical methods, the responses are more accurate and the approximations are lower, but the models are limited to simple geometries. In this regard, Asano (1960) and then, Datta (1974) was among the pioneer researchers who studied the effects of topographic features under *SH*-waves using analytical methods. With the development of the wave function expansion and weighted residual methods, the analytical methods were used in the analysis of underground cavities/tunnels subjected to *SH*-waves by the majority of researchers including Gamer (1977), Lee and Trifunac (1979), Chen (1980), Datta and Shah (1982), Lee and Manoogian (1995), Manoogian (2000), Lee et al. (2002), Wang and Liu (2002), Liu and Lin (2004), Shi et al. (2006), Smerzini et al. (2009), Liang et al. (2010), Tsaur and Chang (2012), Yi et al. (2014), Amornwongpaibun et al. (2016) and Gao et al. (2016). On the other hand, the volumetric numerical methods have been developed for the analysis of underground cavities. Using the finite element method (FEM), Lee and Rowe (1991) and Molinero et al. (2002) presented the ground surface displacement in presence of underground cavities. Utilizing the finite difference method (FDM), Yiouta-Mitra et al. (2007) investigated the importance of underground structures on the seismic response of the ground surface as well as the surface adjacent structures. Also, Besharat et al. (2012) examined the presence of underground structures during an earthquake with regard to Sadr-Niayesh Tunnel as a case study.

In the boundary element method (BEM), one dimension of the models is reduced, the meshes are only concentrated only around the boundary of desired features (the target society of this paper includes subsurface cavities) and the radiation conditions of waves are satisfied at infinity. Therefore, it is an appropriate approach for the dynamic analysis of geotechnical problems (Beskos 1987). The advantages of BEM compared to the volumetric approaches are included the significant reduction in analysis time, lower volume of input data/memory seizure, and large contribution of analytical processes which leads to high precision responses. In full-plane BEM, the model is truncated from a full-space and the boundaries are closed in a distance far away from the desired zone which leads to the approximate satisfaction of stress-free conditions on the ground surface (Ahmad and Banerjee 1988). But, in the half-plane BEM approach, the satisfaction of stress-free boundary condition of the surface is considered in an exact process. Notwithstanding the difficult implementation and creating large equations in the half-plane BEM compared to the full-plane BEM, no discretization of the smooth surface and define fictitious elements for enclosing boundaries is needed. These advantages simplify the modeling process (Panji et al. 2013). Luco, and de-barros, F.C.P. (1994), Yu and Dravinski (2009), Parvanova et al. (2014), and Liu and Liu (2015) were among the researchers who used frequency-domain full-plane BEM to examine the effect of subsurface cavities on the response of ground surface. Also, Benites et al. (1992) determined the seismic response of multiple cavities with the assistance of frequency-domain half-plane BEM. The response of deep and shallow

tunnels subjected to effective loads is presented by Panji et al. 2012and Panji et al. 2016) and Panji and Ansari (2017) using elastostatic full-plane and half-plane BEM, respectively. Because of advantages such as analysis of time-dependent geometries, obtaining the habitude of seismic wave's propagation and obtaining the real solutions, the BEM was developed in the time-domain. The time-domain full-plane BEM was used by Takemiya and Fujiwara (1994) and Kamalian et al. (2008) for analyzing the effects of subsurface topographies. The time-domain half-plane BEM was proposed by some researchers including Rice and Sadd (1984), Belytschko and Chang (1988), and Hirai (1988). Moreover, in the studies of Panji et al. (2013), Panji et al. (2014a, 2014b) and recently, Panji and Mojtabazadeh-Hasanlouei (2018, 2019, 2020), Panji et al. (2020) and Mojtabazadeh-Hasanlouei et al. (2020), they investigated the seismic response of ground surface in the presence of different surface/subsurface topographic features.

In the present paper, the ground surface response was evaluated in the presence of horseshoe-shaped cavity subjected to obliquely propagating incident *SH*-waves using time-domain half-plane BEM. In addition to validate the results compared to existing analytical solutions, the response of the ground surface and the amplification patterns were presented in the time/frequency-domain and the synthetic seismograms were obtained. In this regard, incident wave angle and dimensionless frequency of the responses were studied as the intended parameters. Simple modeling of actual underground structures and obtaining accurate responses through the use of time-domain half-plane BEM were among main purposes of this paper.

2 Time-Domain Half-Plane BEM

Two-dimensional scalar wave equation and governing boundary conditions on the ground surface were respectively introduced for a homogeneous linear elastic medium as follows (Morse and Feshbach 1953; Eringen and Suhubi 1975):

$$\frac{\partial^2 u(x,y,t)}{\partial x^2} + \frac{\partial^2 u(x,y,t)}{\partial y^2} + b(x,y,t) = \frac{1}{c^2}\frac{\partial^2 u(x,y,t)}{\partial t^2}, \qquad (1)$$

$$\mu\frac{\partial u(x,y,t)}{\partial n}\bigg|_{y=0} = 0, \qquad (2)$$

In the above equation, c is the shear wave velocity, $u(x,y,t)$ and $b(x,y,t)$ are the out-of-plane displacement and body forces at coordinates (x,y) and time t, respectively, μ is the shear modulus, and n is the ground surface normal vector. With considering boundary conditions in Eq. (2), the time-domain half-plane fundamental solutions were achieved from singular solution of Eq. (1). After applying the weighted residual integral to Eq. (1) and ignoring body terms and initial conditions, and considering the principles of waves diffraction in a half-plane, the modified direct boundary integral equation (BIE) in time-domain can be obtained as follows (Brebbia and Dominguez 1989; Dominguez 1993):

$$c(\xi)u(\xi,t) = \int_\Gamma \left\{ \int_0^t \left[u^*(x,t;\xi,\tau) \cdot q(x,t) - q^*(x,t;\xi,\tau) \cdot u(x,t) \right] d\tau \right\} d\Gamma(x)$$
$$+ u^{ff}(\xi,t), \tag{3}$$

where u^* is the transient half-plane displacement fundamental solution in the position x and current time t due to an anti-plane single pulse at position ξ and time τ, q^* is the transient half-plane traction fundamental solution obtained from derivative of the displacement fundamental solution along the normal vector, u and q are the boundary displacement and traction values, respectively, $c(\xi)$ is the corner effect, $\Gamma(x)$ is the boundary of the considered domain and u^{ff} is the free-field motion of the ground surface for a uniform and homogeneous half-plane, which also satisfies the stress-free boundary conditions. To solve Eq. (3), it is required to discretize the time-axis and geometric boundary of the body. By discretizing the time-axis in N equal increments and considering linear variations in each time-interval, the temporal integration on the fundamental solutions can be analytically performed (Panji and Mojtabazadeh-Hasanlouei 2018). After forming the spatial integration of Eq. (3) for all BEs, the matrix form of the above equation can be derived as follows:

$$\sum_{n=1}^N H^{N-n+1}\{u^n\} = \sum_{n=1}^N G^{N-n+1}\{q^n\} + \{u^{ff.N}\}, \tag{4}$$

In this equation, $\{u^n\}$ and $\{q^n\}$ are the vectors of boundary nodal quantities at the time-step n. The elements of H^{N-n+1} and G^{N-n+1} can be obtained by integration over the boundary elements. By applying the boundary conditions on the geometric boundaries of the model, the solvable matrix form of Eq. (12) can be achieved as follows:

$$[A_1^1]\{X^N\} = [B_1^1]\{Y^N\} + \{R^N\} + \{u^{ff.N}\}, \tag{5}$$

In which, the vectors or unknown and known boundary variables are illustrated by $\{X^N\}$ and $\{Y^N\}$, respectively and $\{R^N\}$ is the effects of past dynamic-history on the current time-node N.

3 Applications

After converting the above formulation in a general step-by-step time-domain algorithm known as DASBEM (Panji et al. 2013), for validity checks, an underground unlined horseshoe-shaped cavity subjected to *SH*-waves was used as illustrated in Fig. 1. Utilizing time-domain half-plane BEM, only discretizing the boundary of cavity was sufficed the modeling. This problem has been analytically solved by Gao et al. (2016); therefore, was considered for benchmark purposes. DR is the depth ratio of the cavity and fixed on 3 for presented validation examples. Incident wave was assumed as the Ricker wavelet type (Fig. 2) as its function should satisfy the stress-free boundary conditions. The function of a Ricker wavelet type is defined as Eq. (6) (Ricker 1953):
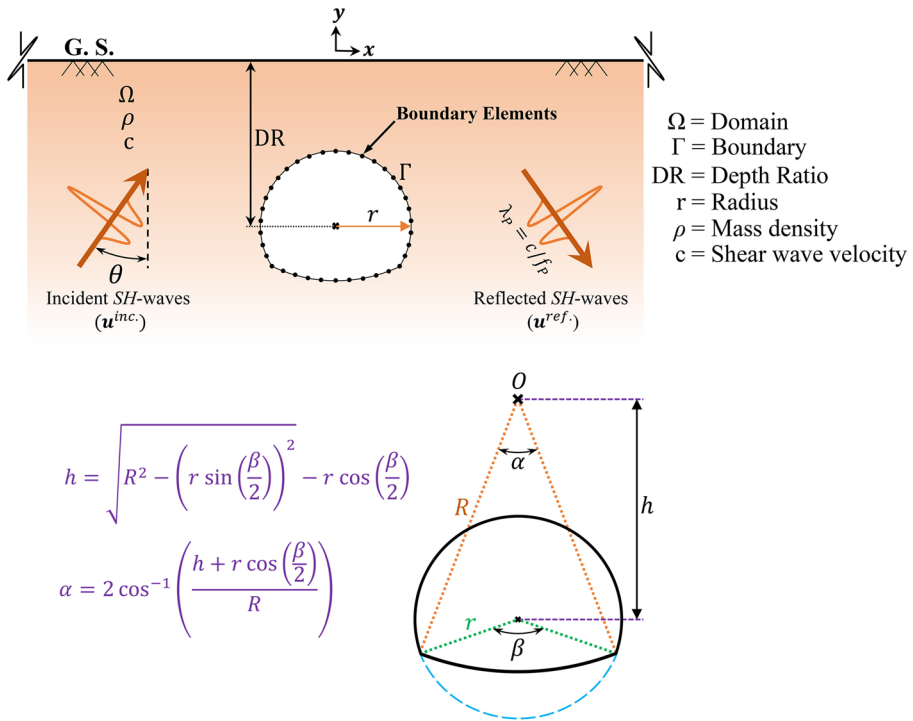
Fig. 1 The problem geometry of a horseshoe-shaped cavity embedded in an elastic half-plane subjected to the incident *SH*-waves

$$f(t) = \left[1 - 2\left(\pi f_p(t-t_0)\right)^2\right] e^{-\left(\pi f_p(t-t_0)\right)^2}, \qquad (6)$$

where f_p is the predominant frequency of the wave and t_0 is the time shifting parameter. The model is embedded in a half-plane and the stress-free boundary conditions of the ground surface are satisfied; Therefore, by adding the phase of the incident and reflected waves, the free-field displacement (u^{ff}) can be obtained as follows (Reinoso et al. 1993):
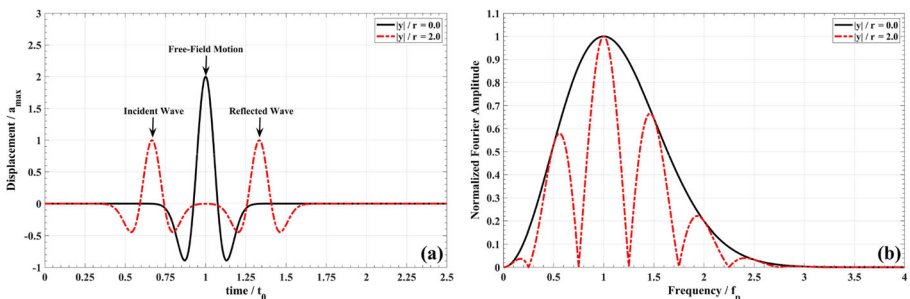

Fig. 2 The Ricker wavelet in the (a) time-domain and (b) frequency-domain

Springer

$$u^{ff}(x,y,t) = \alpha_{max} \cdot \left(\left[1 - 2\left(\frac{\pi f_p}{c}\alpha^{inc.}\right)^2\right] e^{-\left(\frac{\pi f_p}{c}\alpha^{inc.}\right)^2} H\left(t - \frac{r^{inc.}}{c}\right) + \left[1 - 2\left(\frac{\pi f_p}{c}\alpha^{ref.}\right)^2\right] e^{-\left(\frac{\pi f_p}{c}\alpha^{ref.}\right)^2} H\left(t - \frac{r^{ref.}}{c}\right) \right),$$

(7)

in which, α_{max} is the maximum time-history amplitude, $\alpha^{inc.}$ and $\alpha^{ref.}$ are the phase of incident and reflected waves, and H is the Heaviside function. Also, $\alpha^{inc.}$, $\alpha^{ref.}$, $r^{inc.}$ and $r^{ref.}$ can be obtained by the following equations:

$$\alpha^{inc.} = c(t-t_0) + r^{inc.}, \quad r^{inc.} = -\sin(\theta) \cdot x + \cos(\theta) \cdot y,$$

(8)

$$\alpha^{ref.} = c(t-t_0) + r^{ref.}, \qquad r^{ref.} = -\sin(\theta) \cdot x - \cos(\theta) \cdot y,$$

(9)

According to Fig. 1, the nodal distance on the boundary of cavity was assumed equal to 10 and 321 internal points were defined in the surface range (S. R.) of $-4r \leq x \leq 4r$ on the ground surface (G. S.). The problem was solved with 1000 time-steps of 0.01 sec. The predominant frequency, time shift parameter and maximum amplitude of the Ricker wavelet were considered equal to 3 Hz, 2.4 sec., and 0.001 m, respectively. It should be noted that the implementation of numerical procedure has been done in the MATLAB (2020) programming software. The dimensionless frequency can be defined as follows:

$$\eta = \frac{\omega r}{\pi c},$$

(10)

in which, η is the dimensionless frequency, ω is the angular frequency of wave, r is the radius of the cavity, and c is the shear wave velocity. Figures 3 and 4 show the Normalized Displacements Amplitude (NDA) of the ground surface for the dimensionless frequencies of 1 and 4 in the different angles of incident *SH*-wave, compared to analytical solutions of Gao et al. (2016). Based on the mentioned study, the number of coefficients N and M to formulate the analytical solution was equal to 25 and 100, respectively. As can be seen, the results are highly accurate.

3.1 Synthetic Seismograms

Figure 5 shows the general diffraction of the waves on the ground surface in the time-domain subjected to obliquely propagating incident *SH*-wave. In this figure, the surface range of $-4r \leq x \leq 4r$ is considered to obtain the synthetic seismograms. Also, according to the previous section, DR is equal to 3 for all the models. As can be seen in Fig. 5, with increasing the wave angle from 0 degrees (vertically incident wave) to 90 degrees (horizontally incident wave), diffraction of the responses is reduced in location of cavity; But this issue is reverse for peripheral zones ($\pm r \leq x \leq \pm 4r$). Almost, from the fifth second onwards, the responses are converged and rapidly stabled by increasing the incident angle. In other words, fluctuations duration is reduced by increasing θ, so that
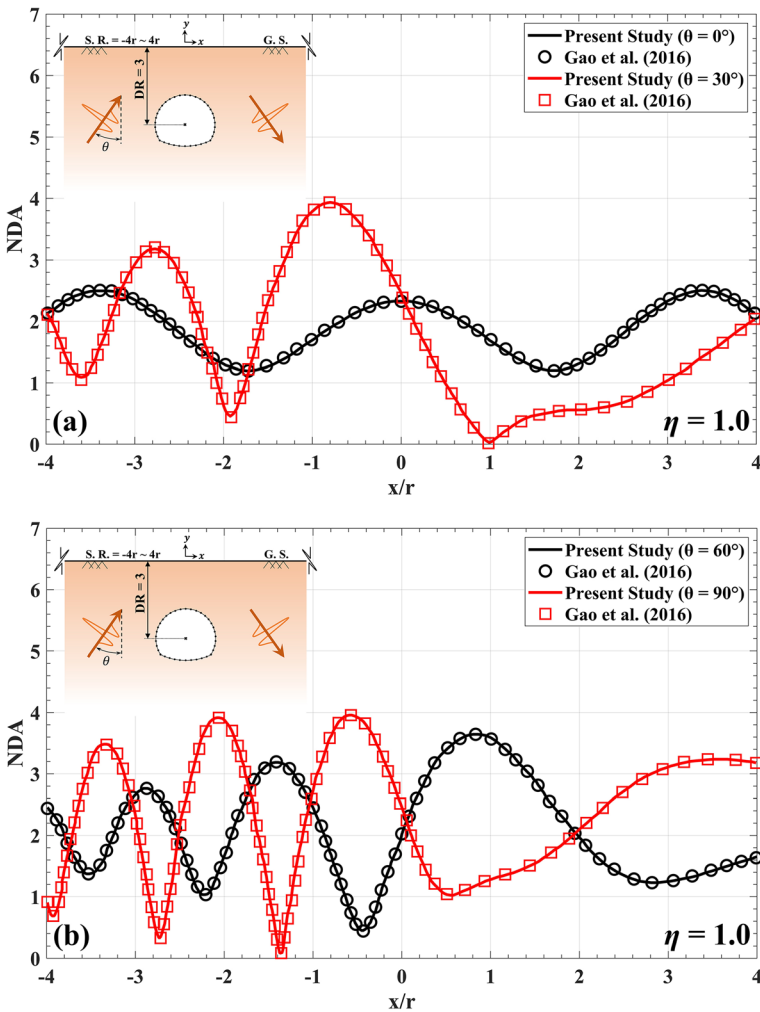
Fig. 3 The normalized displacement amplitude of the ground surface versus x/b for a horseshoe-shaped cavity subjected to the *SH*-waves with the different incident angles and the dimensionless frequency of $\eta = 1.0$

the time-range for vertical and horizontal cases is 1.5 to 3.5 and 1.5 to 3 sec., respectively.

3.2 Amplification Patterns

Although the results presented in the time-domain seem desirable to observe the responses and show waves dispersion, examining the amplification ratio (the ratio of the Fourier amplitude of the response to the Fourier amplitude of the free-field motion) and displaying its behavioral patterns are possible only in the frequency-domain. Thus, Fig. 6 is presented to show the three-dimensional amplification of the ground surface versus the different dimensionless frequencies subjected to obliquely propagating incident *SH*-waves. As shown in this figure, with increasing the dimensionless
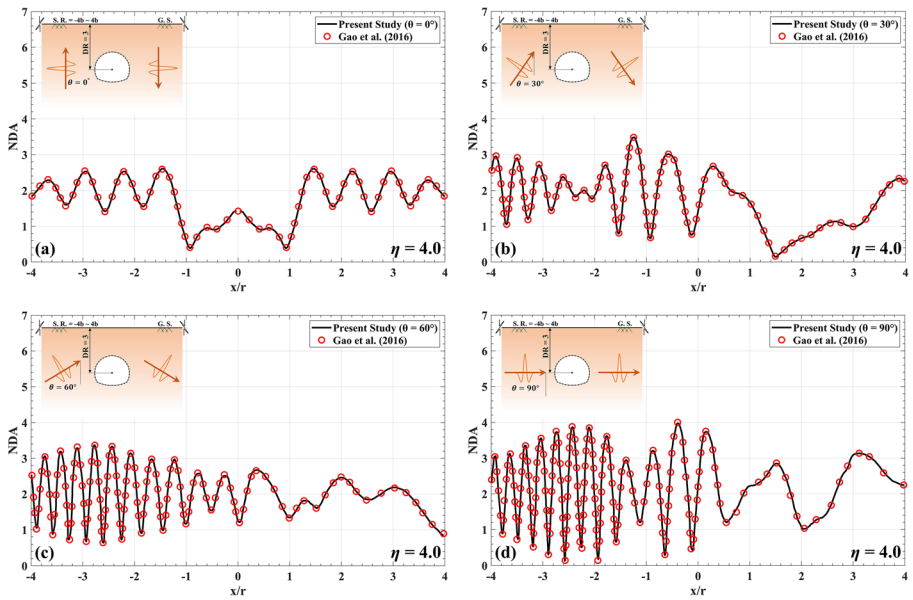
Fig. 4 The normalized displacement amplitude of the ground surface versus x/b for a horseshoe-shaped cavity subjected to the *SH*-waves with the incident angle of (a) $\theta = 0°$, (b) $\theta = 30°$, (c) $\theta = 60°$, and (d) $\theta = 90°$ and the dimensionless frequency of $\eta = 4.0$

frequency, the number of fluctuations, as well as the amplification ratio is increased. Also, the maximum amplification ratio increases with increasing the incident angle of seismic waves. This effect is clarified in a fixed dimensionless frequency (for example, for vertical incident waves, the max amplification is less than 1.5 and for horizontal incident waves, it is more than 2). In the range of ($-r \leq x \leq r$), with inclination of wavefront, the amplification ratio increases and decreases at high and low frequencies, respectively. The effect of isolation related to the presence of cavity is obvious in this range, especially when the incident wave is radiated vertically. With increasing θ, the
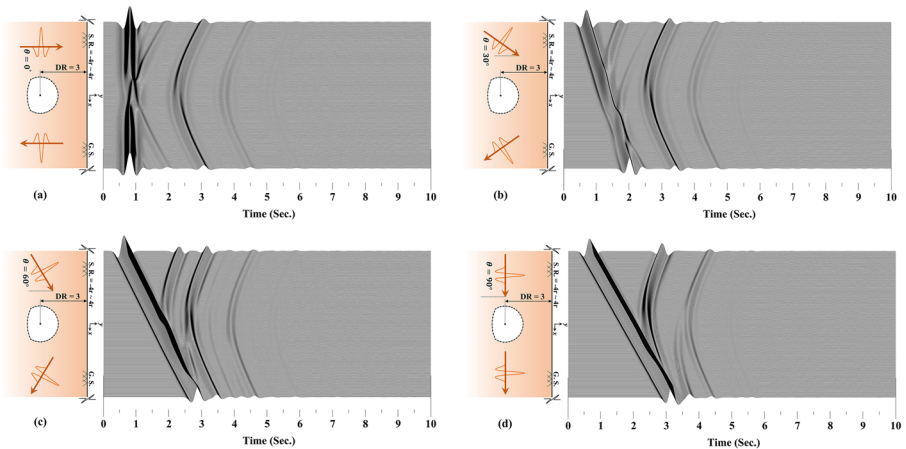

Fig. 5 Synthetic seismograms of the ground surface for a horseshoe-shaped cavity subjected to the *SH*-waves with the incident angle of (a) $\theta = 0°$, (b) $\theta = 30°$, (c) $\theta = 60°$, and (d) $\theta = 90°$
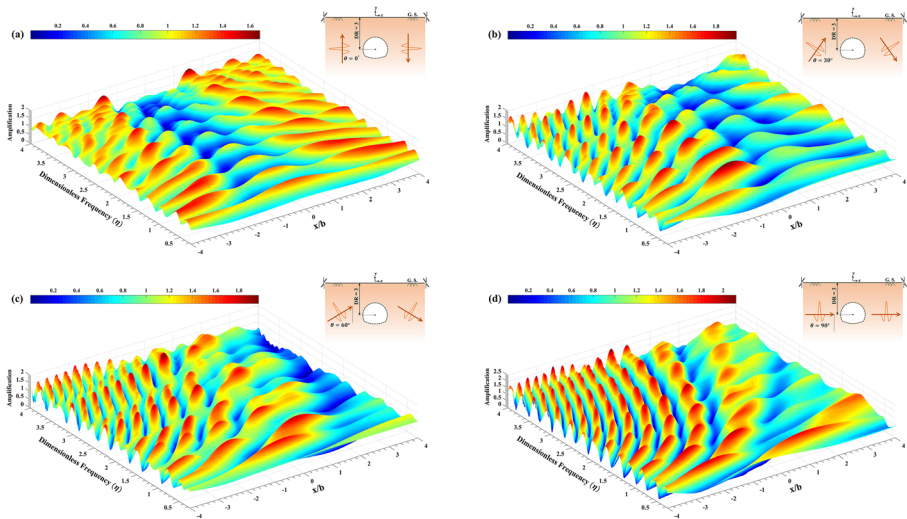
Fig. 6 The 3-D amplification of the ground surface versus different dimensionless frequencies for a horseshoe-shaped cavity subjected to the *SH*-waves with the incident angle of (a) $\theta = 0°$, (b) $\theta = 30°$, (c) $\theta = 60°$, and (d) $\theta = 90°$

turmoil of fluctuations is reduced on the opposite side of the wave-front. To get a better view, Fig. 7 shows the ground surface responses at the different dimensionless frequencies and incident wave angles. As can be seen, with increasing the dimensionless frequency, the number of fluctuations is increased and the maximum responses are observed near the arrival wave-front. According to interest the engineering knowledge for studying the responses in the periodic range of 0.25 to 12 (Borcherdt 1994), which corresponds to the wavelengths based on the width of topographic features, the dimensionless period T is defined as follows:

$$T = \frac{1}{\eta}, \tag{11}$$

According to Fig. 8, to determine the sensitivity of the amplification ratio in different angles of the wave, three stations are considered on the surface to evaluate the amplifications versus dimensionless periods. In this figure, SR is the space ratio between the stations and fixed on 1.5 relative to the central station. As can be seen, however, by increasing the angle of the wave, the maximum/minimum amplification ratio is achieved, but the response reaches stability in less time and converges to the smooth ground surface amplification. Also, it is worth noting that, with increasing the angle of the wave, the number of fluctuations is decreased.

4 Comparative Study

The comparison form of the surface responses in the presence of underground horseshoe and circular-shaped cavities are illustrated in this section. As the results show, the
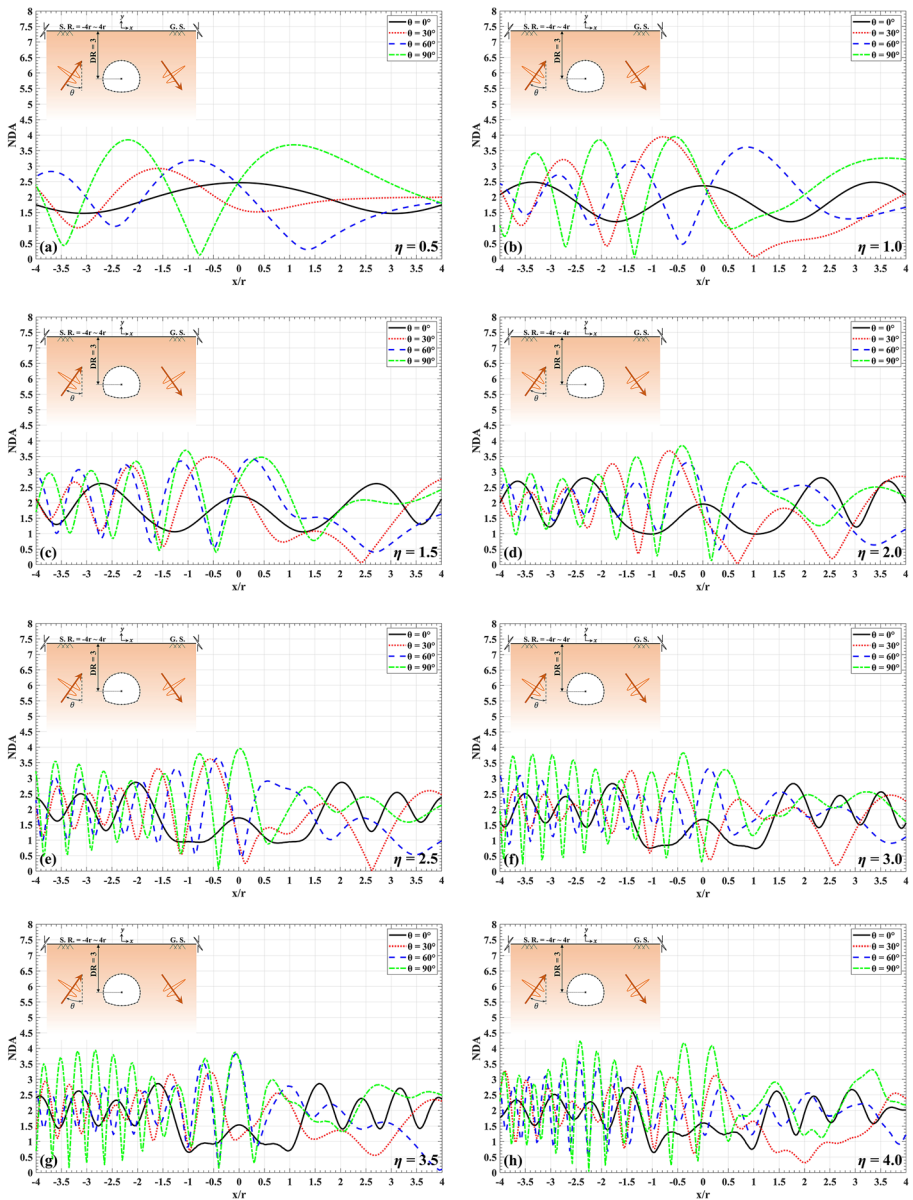
Fig. 7 The normalized displacement amplitude of the ground surface versus x/b for a horseshoe-shaped cavity subjected to the *SH*-waves and the dimensionless frequency of (a) $\eta = 0.5$, (b) $\eta = 1.0$, (c) $\eta = 1.5$, (d) $\eta = 2.0$, (e) $\eta = 2.5$, (f) $\eta = 3.0$, (g) $\eta = 3.5$, and (h) $\eta = 4.0$

amplitude of the reflected waves in the existence of a circular cavity is slightly more than the horseshoe-shaped cavity for the vertical wave-front (Fig. 9). Due to the rotative section of the circular cavity, the seismic waves are more easily crawled/reflected on the boundary of the feature to reach the ground surface; while in the horseshoe-shaped section, its lower boundary acts like a mirror that causes the inverse reflections. But, for
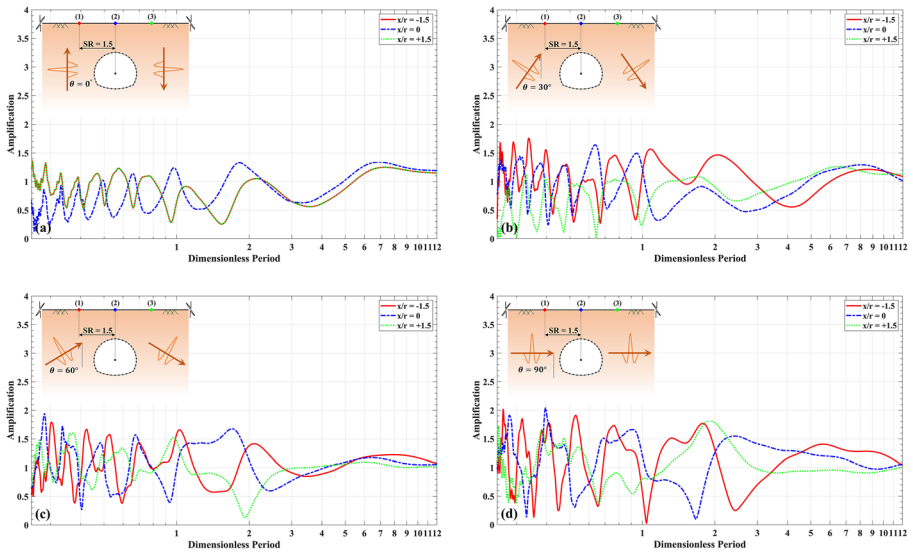
Fig. 8 The amplification of the ground surface versus different dimensionless periods for a horseshoe-shaped cavity subjected to the SH-waves with the incident angle of (a) $\theta = 0°$, (b) $\theta = 30°$, (c) $\theta = 60°$, and (d) $\theta = 90°$
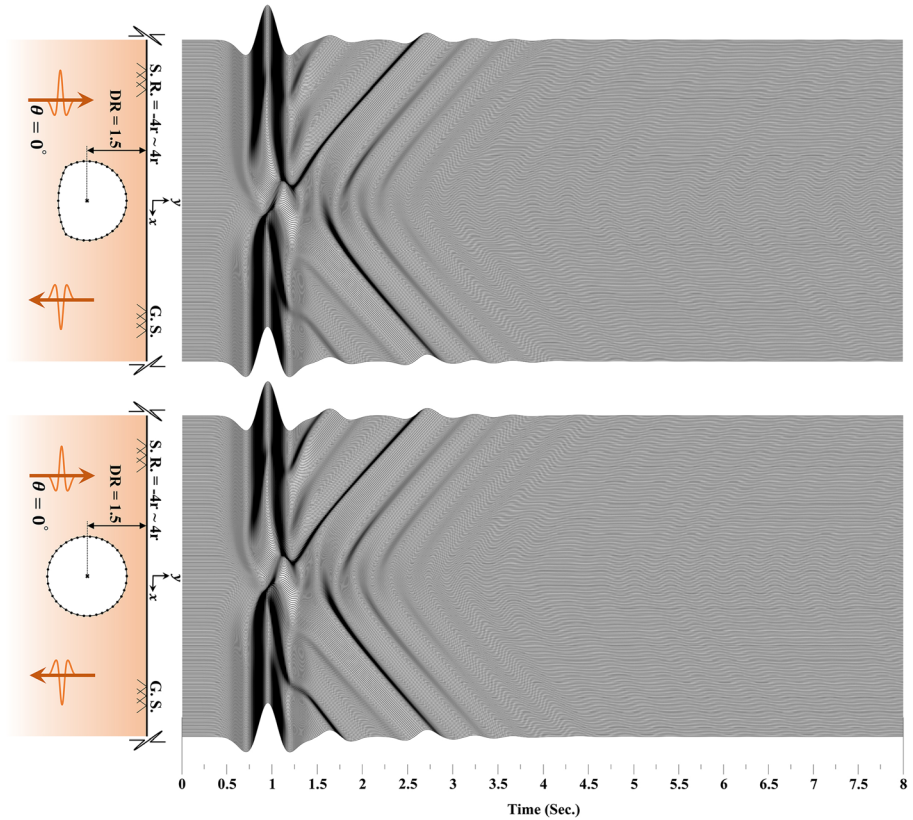

Fig. 9 Comparing the synthetic seismograms of the ground surface for a horseshoe and circular-shaped cavities subjected to the vertical incident SH-waves

horizontal wave-front (Fig. 10), there is no noticeable difference due to the geometry of cavities. By transforming the responses to the frequency domain, the differences become clearer. For vertical and horizontal incidence waves (Figs. 11 and 12), the fluctuations in lateral areas of the horseshoe-shaped cavity are more than the circular case. Moreover, for horizontal wave-font (Fig. 12), the shadow zone effect (Trifunac 1973) is weaker compared to the circular feature. In the following, Figs. 13 and 14 are compared the 2-D displacement of the ground surface in the presence of horseshoe and circular-shaped cavities for dimensionless frequencies of 0.5, 1.0, 1.5, and 2.0. The displacements of the ground surface are determined based on the different depth ratios (DR) of 1.5, 2.5, and 4.5 for vertical and horizontal incidence angles, respectively. As the results show, when the incidence angle is vertical (Fig. 13), the responses of the circular cavity are slightly more than the horseshoe case for different depth ratios, nonetheless, the patterns are in harmony with each other. But, by inclining the wave-front towards the horizon (Fig. 14), the responses of the horseshoe-shaped cavity show a little more displacement. Moreover, there is more agreement between the results before the location of the cavity, where the seismic waves are applied.
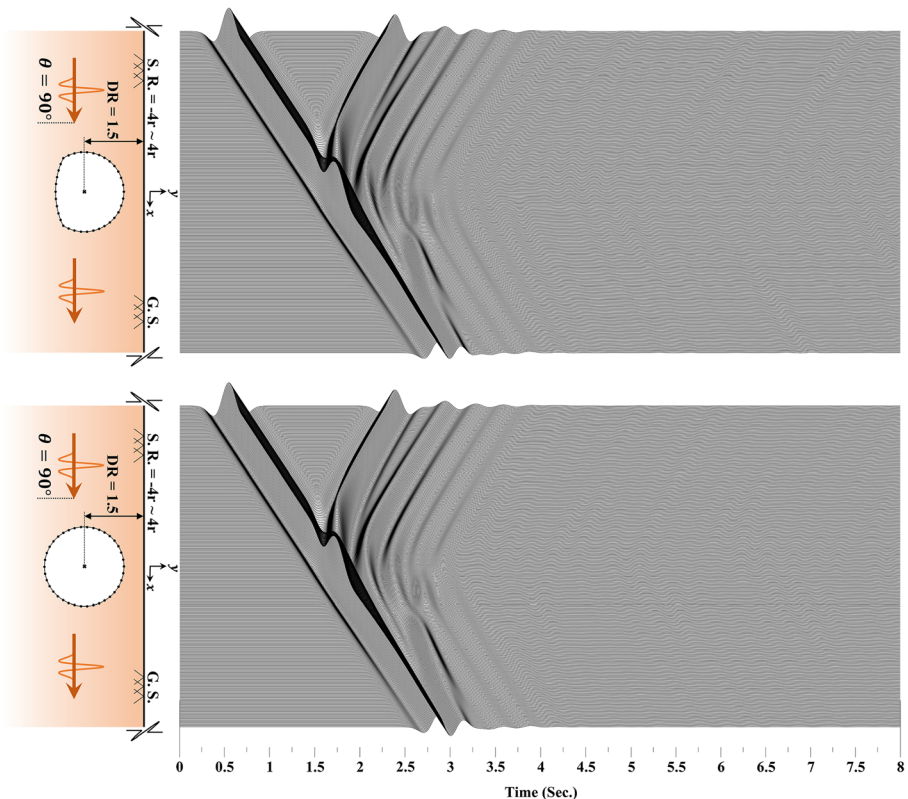

Fig. 10 Comparing the synthetic seismograms of the ground surface for a horseshoe and circular-shaped cavities subjected to the horizontal incident *SH*-waves
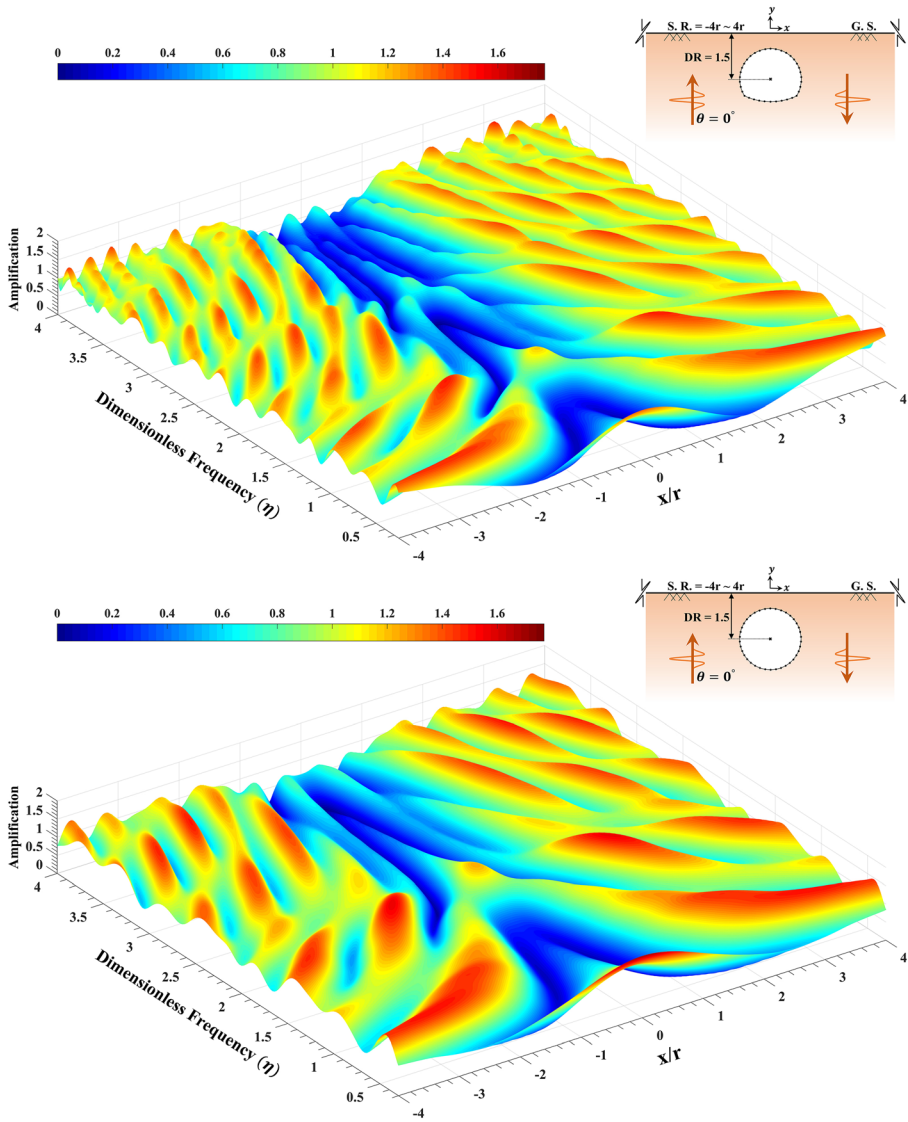
Fig. 11 Comparing the 3-D amplification of the ground surface versus different dimensionless frequencies for a horseshoe and circular-shaped cavities subjected to the vertical incident *SH*-waves

5 Conclusions

A uniform homogenous elastic half-plane medium including a horseshoe-shaped underground cavity was analyzed to determine the seismic response of the ground surface subjected to obliquely propagating incident *SH*-waves. A time-domain half-plane BEM previously proposed by the authors (Panji et al. 2013) was used to create the underground cavity model. Making the meshes focused only on the cavity's surrounding boundary and leaving the discretized ground surface not only reduce the analysis time, but also reduce the input data and calculations volume compared to
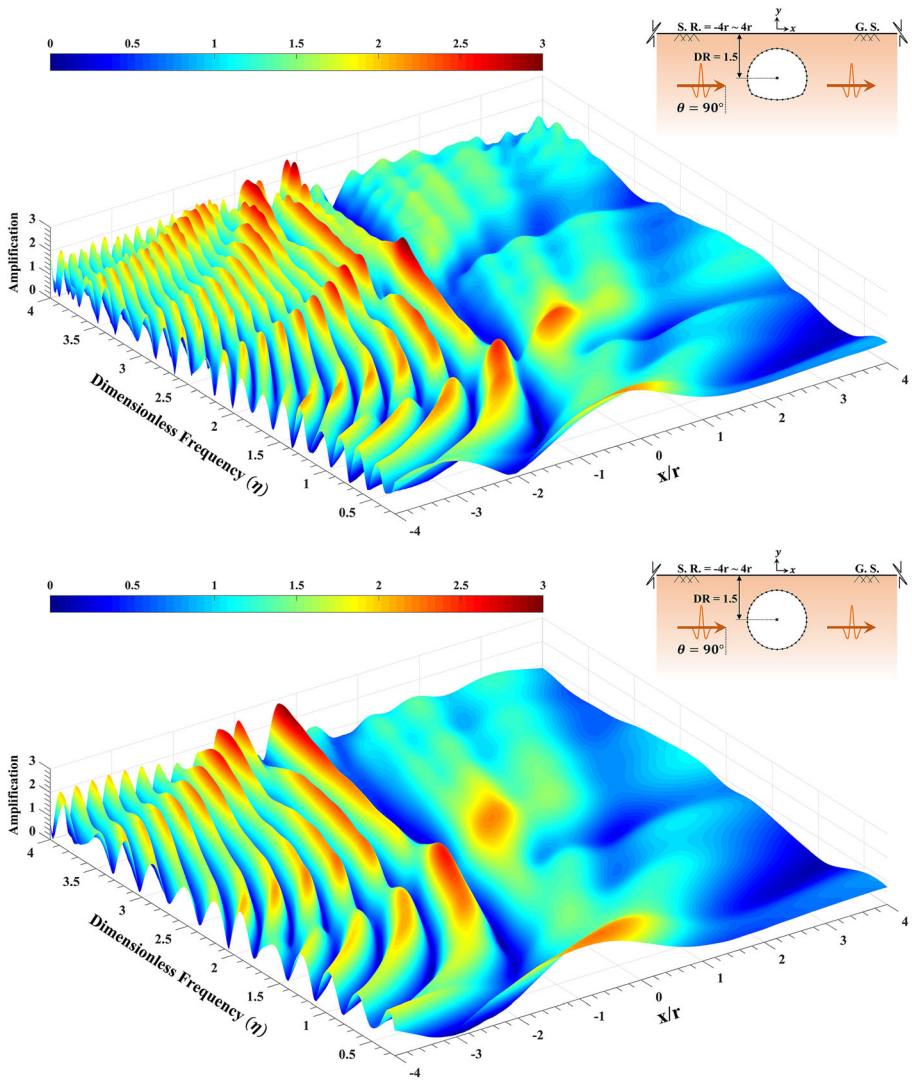
Fig. 12 Comparing the 3-D amplification of the ground surface versus different dimensionless frequencies for a horseshoe and circular-shaped cavities subjected to the horizontal incident *SH*-waves

traditional BEM approaches. The verification of the responses versus existing analytical results showed that the used method had a great accuracy for modeling underground cavities. After the numerical and comparative study, the following results were obtained:

1- As the synthetic seismograms showed, with increasing the angle of incident waves, the convergence occurred earlier and the responses were stabled more quickly.
2- The general pattern of responses in the frequency-domain showed that, when subjected to vertical propagation of incident *SH*-waves, the isolation effect in
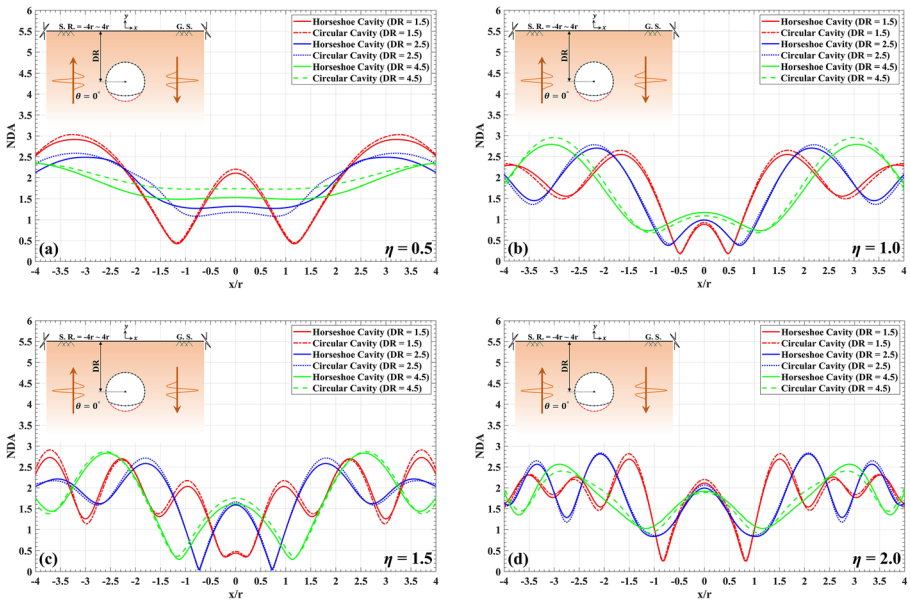
Fig. 13 Comparing the normalized displacement amplitude of the ground surface versus x/b for a horseshoe and circular-shaped cavities subjected to the vertical incident *SH*-waves and the dimensionless frequency of (a) $\eta = 0.5$, (b) $\eta = 1.0$, (c) $\eta = 1.5$ and (d) $\eta = 2.0$

presence of horseshoe-shaped cavity was quite pronounced on reducing the ground surface response.
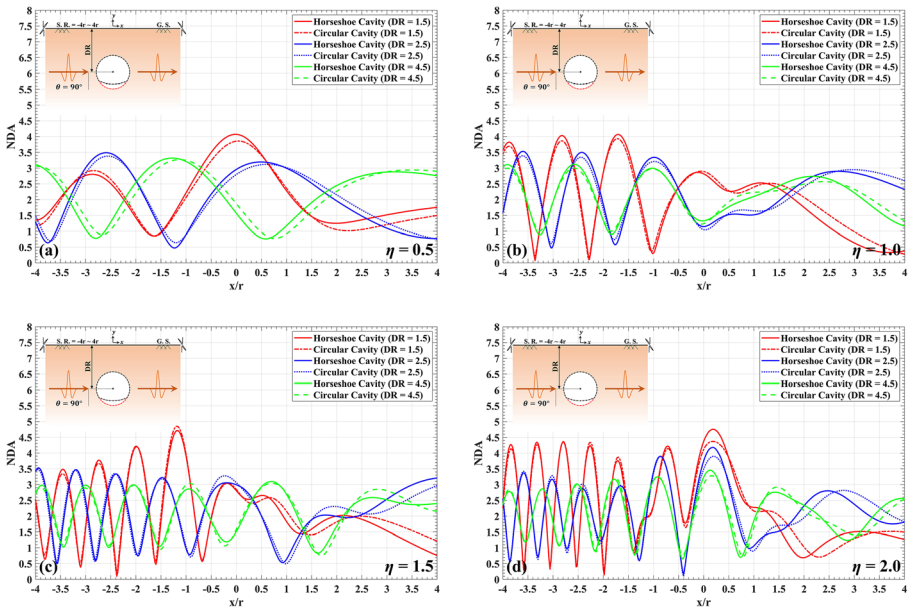

Fig. 14 Comparing the normalized displacement amplitude of the ground surface versus x/b for a horseshoe and circular-shaped cavities subjected to the horizontal incident *SH*-waves and the dimensionless frequency of (a) $\eta = 0.5$, (b) $\eta = 1.0$, (c) $\eta = 1.5$ and (d) $\eta = 2.0$

3- By increasing the angle of incident *SH*-waves, the fluctuations were decreased in the opposite side of the wave-front.

4- By increasing the angle of incident waves for different dimensionless frequencies, the fluctuations of responses continuously increased in the near side of wave-front, directly above the location of cavity.

5- According to the obtained results from the dimensionless period, the responses converged to the amplification of the smooth ground surface (unit value) at the wavelengths that were eight times larger than the feature's width.

6- Comparing the response of horseshoe and circular-shaped cavities showed that the horseshoe case increased the fluctuations in lateral zones and decreased the effect of shadow zone in horizontal incident wave-front.

7- In the vertical incident waves, the response of the circular cavity was slightly more than the horseshoe case, but this procedure was reversed for the horizontal incident wave-front.

References

Ahmad, S., Banerjee, P.K.: Multi-domain BEM for two-dimensional problems of elastodynamics. Int J Numer Methods Eng. **26**(4), 891–911 (1988)

Amornwongpaibun, A., Luo, H., Lee, V.W.: Scattering of anti-plane *SH*-waves by a shallow semi-elliptical hill with a concentric elliptical tunnel. J Earthq Eng. **20**(3), 363–382 (2016)

Asano, S.: Reflection and refraction of elastic waves at a corrugated boundary surface, Part I, The Case of Incidence of *SH*-Wave. Bull Earthq Res Inst. **38**, 177–197 (1960)

Belytschko, T., Chang, H.S.: Simplified direct time integration boundary element method, J Eng Mech. ASCE. **114**(1), 117–134 (1988)

Benites, R., Aki, K., Yomogida, K.: Multiple scattering of *SH*-waves in 2D media with many cavities. Pure Appl Geophys. **138**(3), 353–390 (1992)

Besharat, V., Davoodi, M., Jafari, M.K.: Effect of underground structures on free-field ground motion during earthquakes. In: In 15th World Conference on Earthq Eng. Portugal, Lisbon (2012)

Beskos, D.E.: Boundary element methods in dynamic analysis. Appl Mech Rev. **40**(1), 1–23 (1987)

Borcherdt, R.D.: Estimates of site-dependent response spectra for design (methodology and justification). Earthquake Spectra. **10**(4), 617–653 (1994)

Brebbia, C.A., Dominguez, J.: Boundary Elements, an Introductory Course. Comp Mech Pub, Southampton (1989)

Chen, Y.L.: The analysis of elastic liner in a cylindrical tunnel subjected to *SH*-waves. J Chin Inst Eng. **3**(1), 21–29 (1980)

Datta, S.K.: Diffraction of *SH*-waves by an elliptic elastic cylinder. I J Sol Struct. **10**(1), 123–133 (1974)

Datta, S.K., Shah, A.H.: Scattering of *SH*-waves by embedded cavities. Wave Motion. **4**(3), 265–283 (1982)

Dominguez, J.: Boundary Elements in Dynamics. Comp Mech Publ, Southampton, UK (1993)

Eringen, A.C., Suhubi, E.S.: Elastodynamics. Academic Press, New York (1975)

Gamer, U.: Dynamic stress concentration in an elastic half-space with a semi-circular cavity excited by *SH*-waves. Int J Solids Struct. **13**(7), 675–681 (1977)

Gao, Y., Dai, D., Zhang, N., Wu, Y., Mahfouz, A.H.: Scattering of plane and cylindrical *SH*-waves by a horseshoe shaped cavity. J Earthq Tsu. (2), 1650011, **10** (2016)

Hirai, H.: Analysis of transient response of *SH*-wave scattering in a half-space by the boundary element method. Eng Anal. **5**(4), 189–194 (1988)

Kamalian, M., Jafari, M.K., Ghayamghamian, M.R., Shafiee, A., Hamzehloo, H., Haghshenas, E., Sohrabi-Bidar, A.: Site effect microzonation of Qom, Iran. Eng Geol. **97**(1), 63–79 (2008)

Lee, V.W., Manoogian, M.E.: Surface motion above an arbitrary shape underground cavity for incident *SH*-waves. Eur Earthq Eng. **8**(1), 3–11 (1995)

Lee, K.M., Rowe, R.K.: An analysis of three-dimensional ground movements: The Thunder-Bay tunnel. Can Geotech J. **28**(1), 25–41 (1991)

Lee, V.W., Trifunac, M.D.: Response of tunnels to incident *SH*-waves. J Eng Mech Div. **105**(4), 643–659 (1979)

Lee, V.W., Manoogian, M.E., Chen, S.: Antiplane *SH*-deformations near a surface rigid foundation above a subsurface rigid circular tunnel. Earthq Eng Eng Vib. **1**(1), 27–35 (2002)

Liang, J., Luo, H., Lee, V.W.: Diffraction of plane *SH*-waves by a semi-circular cavity in half-space. Earthq Sci. **23**(1), 5–12 (2010)

Liu, D.K., Lin, H.: Scattering of *SH*-waves by an interacting interface linear crack and a circular cavity near bimaterial interface. Acta Mech Sinica. **20**(3), 317–326 (2004)

Liu, Z., Liu, L.: An IBEM solution to the scattering of plane *SH*-waves by a lined tunnel in elastic wedge space. Earthq Sci. **28**(1), 71–86 (2015)

Luco, J.E., de-barros, F.C.P.: Dynamic displacements and stresses in the vicinity of a cylindrical cavity embedded in a half-space. Earthq Eng Struct Dyn. **23**(3), 321–340 (1994)

Manoogian, M.E.: Scattering and diffraction of *SH*-waves above an arbitrarily shaped tunnel. ISET J Earthq Tech. **37**(1-3), 11–26 (2000)

MATLAB, The language of technical computing. V.9.9. (R2020b) Natick, Massachusetts: The MathWorks Inc (2020)

Mojtabazadeh-Hasanlouei, S., Panji, M., Kamalian, M.: On subsurface multiple inclusions model under transient *SH*-wave propagation. Waves Random Complex Media. 1–40 (2020). https://doi.org/10.1080/17455030.2020.1842553

Molinero, J., Samper, J., Juanes, R.: Numerical modeling of the transient hydrogeological response produced by tunnel construction in fractured bedrocks. Eng Geol. **64**(4), 369–386 (2002)

Morse, P.M., Feshbach, H.: Methods of Theoretical Physics. McGraw-Hill Book Company, McGraw-Hill Book Company, New York (1953)

Panji, M., Ansari, B.: Modeling pressure pipe embedded in two-layer soil by a half-plane BEM. Comput Geotech. **81**, 360–367 (2017)

Panji, M., Mojtabazadeh-Hasanlouei, S.: Time-history responses on the surface by regularly distributed enormous embedded cavities: Incident *SH*-waves. Earthq Sci. **31**, 1–17 (2018)

Panji, M., Mojtabazadeh-Hasanlouei, S.: Seismic amplification pattern of the ground surface in presence of twin unlined circular tunnels subjected to SH-waves [In Persian]. J Transp Infrast Eng. (2019). https://doi.org/10.22075/jtie.2019.16056.1342

Panji, M., Mojtabazadeh-Hasanlouei, S.: Transient response of irregular surface by periodically distributed semi-sine shaped valleys: Incident *SH*-waves. J Earthq Tsu. **14**, 2050005 (2020). https://doi.org/10.1142/S1793431120500050

Panji, M., Asgari-Marnani, J., Tavousi Tafreshi, S.: Evaluation of effective parameters on the underground tunnel stability using BEM. J Struct Eng Geotech. 29–37 (2012)

Panji, M., Kamalian, M., Marnani, J.A., Jafari, M.K.: Transient analysis of wave propagation problems by half-plane BEM. Geophys J Int. **194**(3), 1849–1865 (2013)

Panji, M., Kamalian, M., Marnani, J.A., Jafari, M.K.: Anti-plane seismic response from semi-sine shaped valley above embedded truncated circular cavity: a time-domain half-plane BEM. Int J Civil Eng. **12**(2), 193–206 (2014a)

Panji, M., Kamalian, M., Marnani, J.A., Jafari, M.K.: Analyzing seismic convex topographies by a half-plane time-domain BEM. Geophys J Int. **197**(1), 591–607 (2014b)

Panji, M., Koohsari, H., Adampira, M., Alielahi, H., Marnani, J.A.: Stability analysis of shallow tunnels subjected to eccentric loads by a boundary element method. J Rock Mech Geotech Eng. **8**, 480–488 (2016)

Panji, M., Mojtabazadeh-Hasanlouei, S., Yasemi, F.: A half-plane time-domain BEM for *SH*-wave scattering by a subsurface inclusion. *Comput Geosci*. **134**, 104342 (2020). https://doi.org/10.1016/j.cageo.2019.104342

Parvanova, S.L., Dineva, P.S., Manolis, G.D., Wuttke, F.: Seismic response of lined tunnels in the half-plane with surface topography. Bull Earthq Eng. **12**(2), 981–1005 (2014)

Reinoso, E., Wrobel, L.C., Power, H.: Preliminary results of the modeling of the Mexico City valley with a two-dimensional boundary element method for the scattering of *SH*-waves. Soil Dyn Earthq Eng. **12**(8), 457–468 (1993)

Rice, J.M., Sadd, M.H.: A note on computing elastodynamic full field displacements arising from subsurface singular sources. Mech Res Commun. **11**, 385–390 (1984)

Ricker, N.: The form and laws of propagation of seismic wavelet. Geophys. **18**(1), 10–40 (1953)

Shi, W.P., Liu, D.K., Song, Y.T., Chu, J.L., Hu, A.Q.: Scattering of circular cavity in right-angle planar space to steady *SH*-wave. Appl Math Mech. **27**, 1619–1626 (2006)

Smerzini, C., Aviles, J., Paolucci, R., Sánchez-Sesma, F.J.: Effect of underground cavities on surface earthquake ground motion under *SH*-wave propagation. Earthq Eng Struct Dyn. **38**(12), 1441–1460 (2009)

Takemiya, H., Fujiwara, A.: *SH*-wave scattering and propagation analyses at irregular sites by time-domain BEM. Bull Seismol Soc Am. **84**(5), 1443–1455 (1994)

Trifunac, M.D.: Scattering of plane *SH*-waves by a semi-cylindrical canyon. Earthq Eng Struct Dyn. **1**, 267–281 (1973)

Tsaur, D.H., Chang, K.H.: Multiple scattering of *SH*-waves by an embedded truncated circular cavity. J Mar Sci Technol. **20**(1), 73–81 (2012)

Wang, G., Liu, D.: Scattering of *SH*-wave by multiple circular cavities in half-space. Earthq Eng Eng Vib. **1**(1), 36–44 (2002)

Yi, C., Zhang, P., Johansson, D., Nyberg, U.: Dynamic analysis for a circular lined tunnel with an imperfectly bonded interface impacted by plane *SH*-waves, Proceedings of the World Tunnel Congress 2014-Tunnels for a better Life. Foz do Iguaçu, Brazil (2014)

Yiouta-Mitra, P., Kouretzis, G., Bouckovalas, G., Sofianos, A.: Effect of underground structures in earthquake resistant design of surface structures. Dyn Resp Soil Proper. 1–10 (2007)

Yu, M.C., Dravinski, M.: Scattering of a plane harmonic *SH*-wave by a completely embedded corrugated scatterer. Int J Numer Methods Eng. **78**, 196–214 (2009)

Terms and Conditions

Springer Nature journal content, brought to you courtesy of Springer Nature Customer Service Center GmbH ("Springer Nature").

Springer Nature supports a reasonable amount of sharing of research papers by authors, subscribers and authorised users ("Users"), for small-scale personal, non-commercial use provided that all copyright, trade and service marks and other proprietary notices are maintained. By accessing, sharing, receiving or otherwise using the Springer Nature journal content you agree to these terms of use ("Terms"). For these purposes, Springer Nature considers academic use (by researchers and students) to be non-commercial.

These Terms are supplementary and will apply in addition to any applicable website terms and conditions, a relevant site licence or a personal subscription. These Terms will prevail over any conflict or ambiguity with regards to the relevant terms, a site licence or a personal subscription (to the extent of the conflict or ambiguity only). For Creative Commons-licensed articles, the terms of the Creative Commons license used will apply.

We collect and use personal data to provide access to the Springer Nature journal content. We may also use these personal data internally within ResearchGate and Springer Nature and as agreed share it, in an anonymised way, for purposes of tracking, analysis and reporting. We will not otherwise disclose your personal data outside the ResearchGate or the Springer Nature group of companies unless we have your permission as detailed in the Privacy Policy.

While Users may use the Springer Nature journal content for small scale, personal non-commercial use, it is important to note that Users may not:

1. use such content for the purpose of providing other users with access on a regular or large scale basis or as a means to circumvent access control;

2. use such content where to do so would be considered a criminal or statutory offence in any jurisdiction, or gives rise to civil liability, or is otherwise unlawful;

3. falsely or misleadingly imply or suggest endorsement, approval , sponsorship, or association unless explicitly agreed to by Springer Nature in writing;

4. use bots or other automated methods to access the content or redirect messages

5. override any security feature or exclusionary protocol; or

6. share the content in order to create substitute for Springer Nature products or services or a systematic database of Springer Nature journal content.

In line with the restriction against commercial use, Springer Nature does not permit the creation of a product or service that creates revenue, royalties, rent or income from our content or its inclusion as part of a paid for service or for other commercial gain. Springer Nature journal content cannot be used for inter-library loans and librarians may not upload Springer Nature journal content on a large scale into their, or any other, institutional repository.

These terms of use are reviewed regularly and may be amended at any time. Springer Nature is not obligated to publish any information or content on this website and may remove it or features or functionality at our sole discretion, at any time with or without notice. Springer Nature may revoke this licence to you at any time and remove access to any copies of the Springer Nature journal content which have been saved.

To the fullest extent permitted by law, Springer Nature makes no warranties, representations or guarantees to Users, either express or implied with respect to the Springer nature journal content and all parties disclaim and waive any implied warranties or warranties imposed by law, including merchantability or fitness for any particular purpose.

Please note that these rights do not automatically extend to content, data or other material published by Springer Nature that may be licensed from third parties.

If you would like to use or distribute our Springer Nature journal content to a wider audience or on a regular basis or in any other manner not expressly permitted by these Terms, please contact Springer Nature at

onlineservice@springernature.com